

Right-handed neutrino production through first-generation leptoquarks

Gokul Duraikandan,^{1,*} Rishabh Khanna,^{2,†} Tanumoy Mandal,^{1,‡} Subhadip Mitra,^{2,3,§} and Rachit Sharma^{1,¶}

¹Indian Institute of Science Education and Research Thiruvananthapuram, Vithura, Kerala, 695 551, India

²Center for Computational Natural Sciences and Bioinformatics,

International Institute of Information Technology, Hyderabad 500 032, India

³Center for Quantum Science and Technology, International Institute of Information Technology, Hyderabad 500 032, India

The collider phenomenology of leptoquarks (LQs) and right-handed neutrinos (RHNs) has been studied extensively in the literature. Because of the gauge singlet nature, the production of RHNs at the LHC is typically suppressed by the tiny light-heavy neutrino mixing angles. In this study, we explore a promising scenario where the presence of an LQ mediator significantly enhances RHN production. We focus on first-generation scalar and vector LQs interacting with the first-generation RHN. The prospects are better for the first-generation scenario than the other generations because of the enhanced parton distribution functions (PDFs) of first-generation quarks. The enhanced PDFs boost the production cross sections of LQs, particularly their single and indirect productions. Incorporating all production modes of LQs that result in a pair of RHNs, we estimate the discovery prospects by analysing the monoelectron and dielectron channels arising from the decay of the RHN pair. We find that the indirect production of LQs is crucial in determining the discovery reach at the HL-LHC for the first-generation scenario.

I. INTRODUCTION

Contemporary experimental advancements have significantly refined the measurements in the neutrino sector, establishing that at least two neutrino states possess tiny but nonzero masses (~ 0.1 eV). These findings have inspired various theoretical constructions to account for the origins of the observed masses and mixing. The type-I seesaw mechanism [1, 2] shows a simple way to generate nonzero neutrino masses by introducing heavy right-handed neutrinos (RHNs). To achieve sub-eV light neutrinos, in this case, the Majorana mass scale (Λ_M) of the RHNs must be very high—around the grand unification scale for Yukawa couplings of order unity. This renders the RHNs inaccessible at TeV-scale colliders like the LHC. A Yukawa coupling of order 10^{-6} could bring Λ_M down to the TeV range, but, in this case, the RHNs would be long-lived and might decay outside the detectors. The inverse seesaw mechanism (ISM) [3, 4], on the other hand, shows promise from the collider perspective, for it naturally contains TeV-scale RHNs that decay promptly, making them detectable at colliders.

Because of their gauge singlet nature, RHN productions at colliders are highly suppressed by the small light-heavy neutrino mixing angle. (Current constraints on the RHN mass and mixing angles are discussed in Ref. [5], while prospects for heavy RHN searches at future lepton colliders are discussed in Ref. [6].) An interesting possibility for RHN production arises from the decays of other beyond the Standard Model (SM) particles, such as W' bosons [7–9], Z' bosons [10–17], or leptoquarks (LQs or ℓ_q) [18, 19], etc. Since, in these cases, the production is no longer dependent on the active-sterile mixing, they can be produced easily. From the LHC perspective, the production

via TeV-scale LQs looks particularly promising [19]. LQs are hypothetical coloured bosons (scalar or vector) carrying both baryon and lepton numbers. Consequently, they bridge the baryon and lepton sectors, enabling couplings between quarks and the RHNs. LQs naturally emerge in various extensions of the SM aiming to unify matter or forces. They are integral to a wide range of theoretical frameworks beyond the SM, such as the Pati-Salam model [20, 21], Grand Unified Theories [22, 23], composite models [24], coloured Zee-Babu models [25], technicolor models [26, 27] and Supersymmetry with R -parity violation [28]. Recently, LQs garnered significant attention in the literature as potential explanations for various low-energy anomalies [29–31].

Previously, we studied the production of RHNs through second-generation LQs at the LHC [19]. Here, we focus on RHN productions via first-generation LQs. These LQs couple to a first-generation quark and the first-generation RHN, whose decay produces a first-generation lepton in the final state. For our collider study, we assume a TeV-range first-generation LQ decays exclusively to a lighter first-generation RHN at the tree level, i.e., the branching ratio (BR) of the $\ell_q \rightarrow q\nu_R$ decay is essentially 100%. At the LHC, RHN pairs can be produced through all three LQ production mechanisms [19]: LQ pair and single productions (P- and SPs) where the LQs decay to the RHN, and the t -channel LQ exchange ($pp \rightarrow \nu_R \nu_R$), or LQ indirect production (IP) [32]. The LQ generation strongly influences the single and indirect production cross sections, as the quark parton distribution functions (PDFs) vary significantly across generations. As a result, the first-generation case requires a separate study from the second-generation one, even though the detection efficiencies of the first and second-generation leptons (i.e., e and μ) are not significantly different. However, the third-generation case differs from those of the first two generations both in terms of initial-quark PDFs and the detection strategies of the final states. We plan to address the third-generation case in a separate study.

If a LQ decays predominantly to the RHN, it is not bound by any direct or indirect collider constraints—the LHC has

* gokulduraikandan19@iisertvm.ac.in

† rishabh.khanna@research.iiit.ac.in

‡ tanumoy@iisertvm.ac.in

§ subhadip.mitra@iiit.ac.in

¶ rachit21@iisertvm.ac.in

TABLE I. List of LQs and their representations under the SM gauge groups. In the second column, we show the representations under $SU(3)_C$, $SU(2)_L$ and $U(1)_Y$, respectively. In the last column, we present the LQ interactions with ν_R [33].

LQ	$(SU(3)_C, SU(2)_L, U(1)_Y)$	Spin	Interaction Lagrangian
\mathbf{S}_1	$(\bar{\mathbf{3}}, 1, 1/3)$	0	$y_{1ij}^{LL} \bar{Q}_L^{ci,a} S_1 \epsilon^{ab} L_L^{j,b} + y_{1ij}^{RR} \bar{u}_R^i S_1 e^j + \bar{y}_{1ij}^{RR} \bar{d}_R^i S_1 \nu_R^j + \text{h.c.}$
$\bar{\mathbf{S}}_1$	$(\bar{\mathbf{3}}, 1, -2/3)$	0	$\bar{y}_{1ij}^{RR} \bar{u}_R^i \bar{S}_1 \nu_R^j + \text{h.c.}$
$\tilde{\mathbf{R}}_2$	$(\mathbf{3}, 2, 1/6)$	0	$-\bar{y}_{2ij}^{RL} \bar{d}_R^i \tilde{R}_2^a \epsilon^{ab} L_L^{j,b} + \bar{y}_{2ij}^{LR} \bar{Q}_L^{i,a} \tilde{R}_2^a \nu_R^j + \text{h.c.}$
\mathbf{U}_1	$(\mathbf{3}, 1, 2/3)$	1	$\mathcal{L} \supset x_{1ij}^{LL} \bar{Q}_L^{i,a} \gamma^\mu U_{1,\mu} L_L^{j,a} + x_{1ij}^{RR} \bar{d}_R^i \gamma^\mu U_{1,\mu} e^j + x_{1ij}^{RR} \bar{u}_R^i \gamma^\mu U_{1,\mu} \nu_R^j + \text{h.c.}$
$\bar{\mathbf{U}}_1$	$(\mathbf{3}, 2, -1/3)$	1	$\bar{x}_{1ij}^{RR} \bar{d}_R^i \gamma^\mu \bar{U}_{1,\mu} \nu_R^j + \text{h.c.}$
$\tilde{\mathbf{V}}_2$	$(\bar{\mathbf{3}}, 1, -1/6)$	1	$\bar{x}_{2ij}^{RL} \bar{u}_R^i \gamma^\mu \tilde{V}_{2,\mu}^b \epsilon^{ab} L_L^{j,a} + \bar{x}_{2ij}^{LR} \bar{Q}_L^{i,a} \gamma^\mu \epsilon^{ab} \tilde{V}_{2,\mu}^b \nu_R^j + \text{h.c.}$

yet to probe and constrain this part of the LQ parameter space. The RHN production through LQ decay becomes significant when neither of these particles is too heavy and the RHN is lighter than the LQ. Since LQs are strongly interacting particles, they can be abundantly produced at the LHC, enhancing the RHN production. The cross section of this process mainly depends on a few parameters like the RHN and LQ masses, the RHN-LQ-quark couplings, and the PDFs of the initial partons. The cross section of the $qq \rightarrow \nu_R \nu_R$ process through a t -channel LQ exchange is proportional to the fourth power of the RHN-LQ-quark couplings. Hence, this coupling can not be small for the IP-mediated process to be significant.

In this paper, we analyse RHN production through all the above-mentioned channels at the LHC. The plan of the paper is as follows. In the next section, we list the LQ models with RHN decay mode. In Section III, we discuss various possible final states arising from the decay of a pair of RHN that can be searched for at the HL-LHC. We also discuss the SM backgrounds and selection criteria for the monoelectron and dielectron channels. We present our findings in Section IV and conclude in Section V.

II. LEPTOQUARK MODELS

We consider all possible LQs that simultaneously interact with a first-generation quark and a RHN. Table I shows the scalar and vector LQs (sLQs and vLQs) with the necessary couplings. Since we are only interested in the collider phenomenology of these models, we ignore the diquark operators to bypass the proton-decay restrictions. Following Ref. [33], we denote the Yukawa coupling matrices of scalar and vector LQs with quark-lepton pairs generically as y and x , respectively. The first subscript of the couplings indicates the $SU(2)_L$ representation and the superscripts indicate the chiralities of the fermions (the first one denotes the quark chirality and the second one, the lepton chirality). For

simplicity, we assume both Pontecorvo-Maki-Nakagawa-Sakata (PMNS) neutrino-mixing and Cabibbo-Kobayashi-Maskawa (CKM) quark-mixing matrices to be approximately equal to unity. This is justified since, unlike the second-generation case [19], the cross sections of the processes initiated by the first-generation quarks are not affected significantly by the presence of the small off-diagonal terms in the quark-mixing matrix, and the LHC experiments cannot identify the flavour of the missing neutrinos. Vector LQs can have an extra gluon coupling allowed by the gauge symmetries that can affect their productions at the LHC [34, 35]:

$$\mathcal{L} \supset -ig_s(1 - \kappa) \chi_\mu^\dagger T^a \chi_\nu G^{a\mu\nu} \quad (1)$$

where $\chi_{\mu\nu}$ denotes the field strength tensor of a generic vLQs χ and $G^{a\mu\nu}$ denotes the field strength tensor of the gluon.

III. LHC PHENOMENOLOGY

We incorporate the new physics Lagrangian in FEYNRULES [42] to produce the model files for further simulation. We use MADGRAPH5 [43] to generate the leading-order signal and background events with the NNPDF23LO1 [44] PDF set using the default dynamical scale setting. Where available, we use appropriate K_{QCD} factors to account for higher-order cross sections. In the signal, we use an average NLO QCD K factor of 1.58 [45–50] for the sLQ pair production. The events are passed through PYTHIA8 [51] (for hadronization and showering) and DELPHES3 [52] (for detector simulation using the standard CMS card). We use FASTJET's anti-clustering algorithm [53, 54] to reconstruct the jets from the DELPHES tower objects. In our study, we use jets with two radii: (a) jets with $R = 0.4$ (we call this an AK4 jet and denote it as j) and (b) fatjet with $R = 1.2$ (denoted by J). We denote light leptons with $\ell = \{e, \mu\}$.

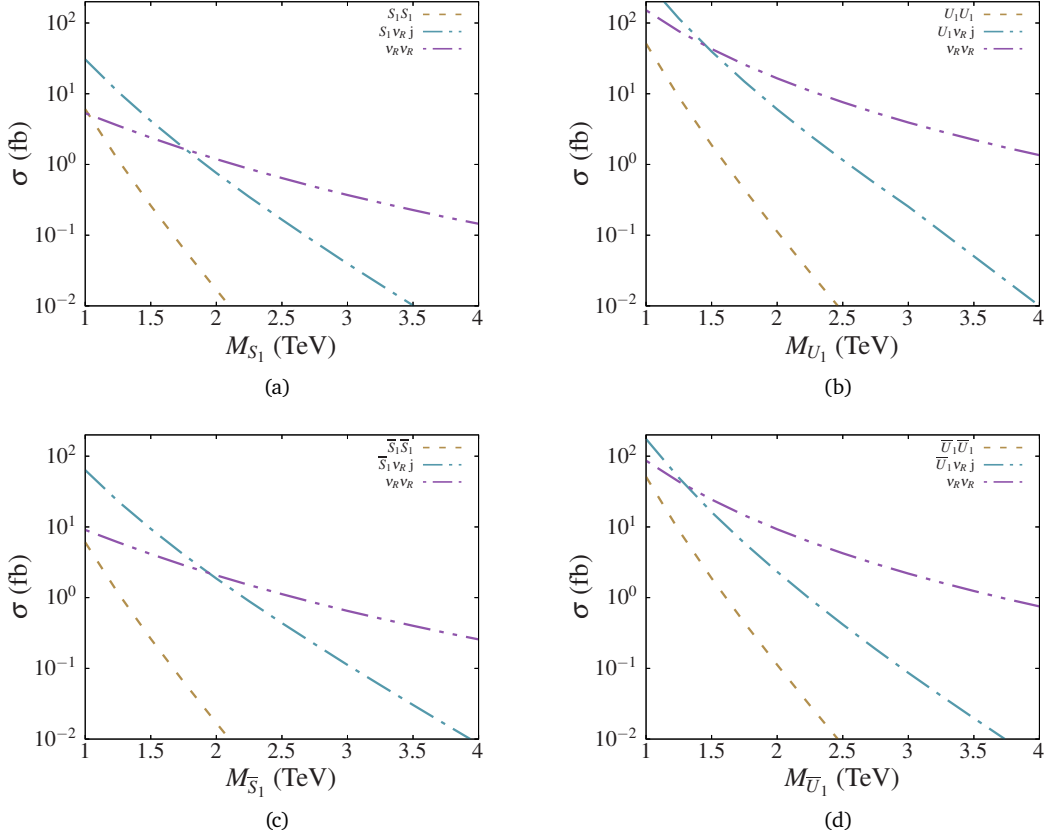


FIG. 1. Cross sections of various production modes of charge-2/3 and 1/3 sLQs (left) and vLQs (right) at the 14 TeV LHC. For these plots, we set $M_{\nu_R} = 500$ GeV and $x/y = 1$. The vLQ plots are obtained for $\kappa = 1$.

TABLE II. Higher-order cross sections of the major background processes without decay and any cut. Their QCD orders are shown in the last column. We use these cross sections to compute the K factors to incorporate the higher-order effects.

Background processes		σ (pb)	QCD order
V+ jets [36, 37]	Z+ jets	6.33×10^4	N ² LO
	W+ jets	1.95×10^5	NLO
VV+ jets [38]	WW+ jets	124.31	NLO
	WZ+ jets	51.82	NLO
	ZZ+ jets	17.72	NLO
	tW	83.10	N ² LO
Single t [39]	tb	248.00	N ² LO
	tj	12.35	N ² LO
tt [40]	tt + jets	988.57	N ³ LO
ttV [41]	ttZ	1.05	NLO+N ² LL
	ttW	0.65	NLO+N ² LL

A. Production at the LHC

Two LQs can be pair-produced via pure QCD or QED interactions, a mixture of QCD-QED interactions, or the RHN-

LQ-quark couplings (x/y). In SP, a single LQ is produced in association with a RHN, primarily mediated by the new coupling x/y . In IP, a LQ is exchanged in the t -channel, producing two RHNs. In the high-mass region, the non-resonant production of LQs surpasses their resonant productions when the new coupling(s) involved is(are) sufficiently large. While the PP cross section remains largely insensitive to the LQ couplings as long as they are not too large, the SP and IP cross sections scale as the second and fourth powers of these couplings, respectively. The generation of the initial quarks also affects these cross sections. The IP is more significant in this case than in the case of second-generation LQs [19] because of relatively larger PDFs of the first-generation quarks.

In this analysis, we focus on first-generation LQs with $M_{\ell q} > M_{\nu_R}$, enabling LQs to decay into RHNs and jets. We assume that LQs decay exclusively to RHNs, meaning the branching ratio (BR) for the $\ell q \rightarrow \nu_R q$ channel is 100%. All three production modes of LQs result in the production of a pair of RHNs accompanied by jets. For the PP and SP, the accompanied jets arise from the decay of LQ, whereas in the case of the IP, jets arise from radiation. We further assume that the RHN mass is a few hundred GeV, allowing them to decay resonantly into the $W\ell$, $Z\nu$, and $H\nu$ channels (with branching ratios (BRs) approximately in the 2 : 1 : 1 proportion). Based on the various possible combinations of $\nu_R \nu_R$ decays, we identify the following

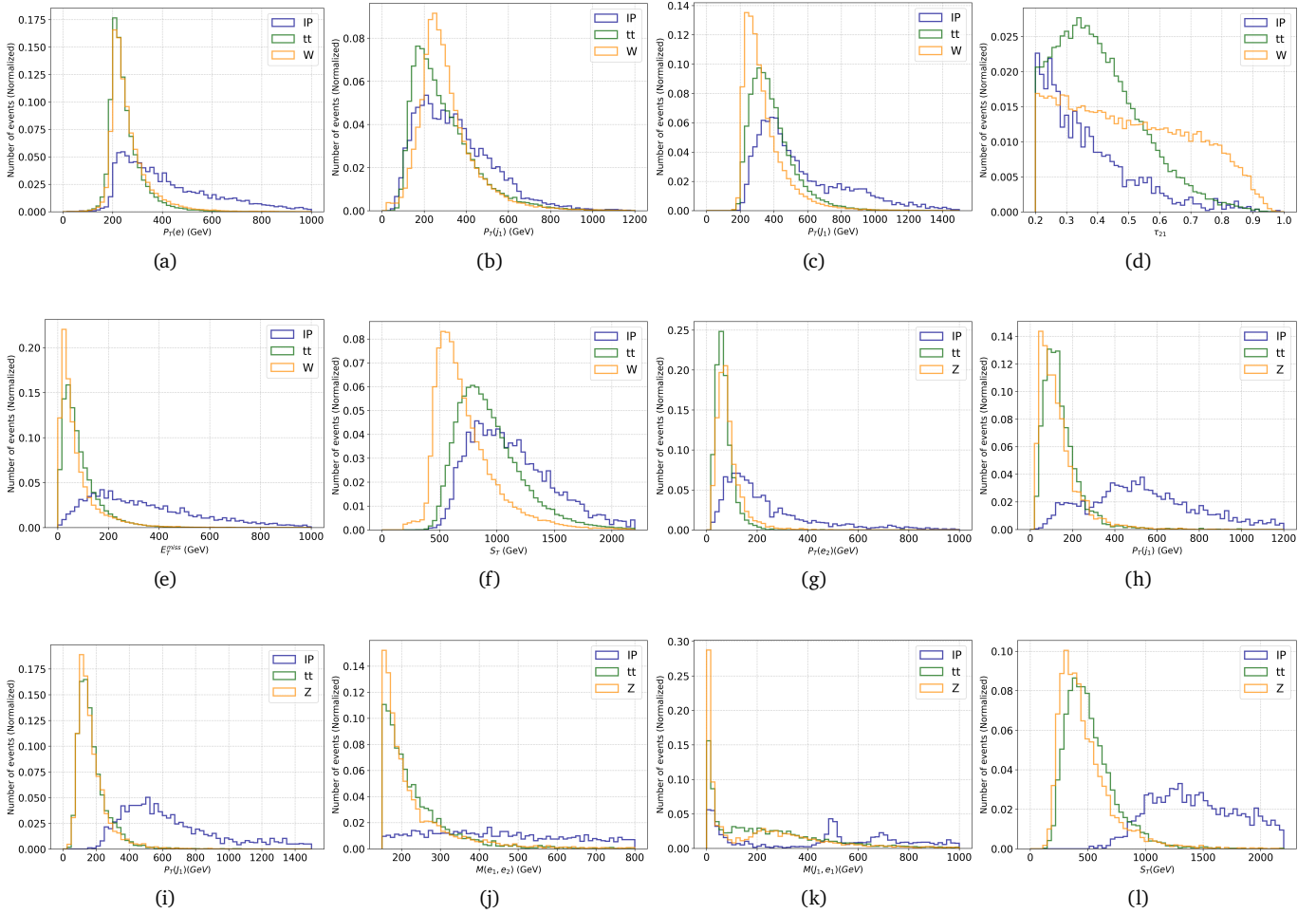


FIG. 2. Normalised distributions of various kinematic variables for the signal and two dominant backgrounds in both the monoelectron and dielectron final states. The benchmark point for the signal used here is $(M_{\ell q}, M_{\nu R}) = (2.5 \text{ TeV}, 0.5 \text{ TeV})$. For the monoelectron case [(a)–(f)], the dominant backgrounds are W_e and $t_e t_h$, while for the dielectron case [(g)–(l)], they are Z_e and $t_e t_e$.

final-state categories.

Monolepton: A single lepton in the final state can arise when one ν_R decays via the $W\ell$ channel, while the other ν_R decays via the $Z\nu_\ell$ or $H\nu_\ell$ channel. This final state also includes missing transverse energy. Additionally, hadronic decays of the Z and H bosons can produce fatjets. The various production channels contributing to monolepton final states are as follows:

$$pp \rightarrow \left\{ \begin{array}{l} \ell_q \ell_q \\ \ell_q \nu_R (+j) \\ \nu_R \nu_R (+j) \end{array} \right\} \rightarrow \left\{ \begin{array}{l} (j\nu_R)(j\nu_R) \\ (j\nu_R)\nu_R (+j) \\ \nu_R \nu_R (+j) \end{array} \right\} \\ \rightarrow \ell^\pm W_h^\mp \nu_\ell (Z_h + H_h) + \text{jet}(s).$$

Here, the subscript h stands for the hadronic decay mode of the associated particle. The most dominant channel is when a pair of RHN decays through $\nu_R \nu_R \rightarrow \ell^\pm W_h^\mp \nu_\ell Z_h/H_h$, with an overall BR of 23%. The second most dominant channel, $\nu_R \nu_R \rightarrow \ell^\pm W_h^\mp \nu_\ell Z_\nu$, has a branching ratio (BR) of 7%. However, its contribution to the results is minimal due to low efficiency from selection cuts. All other channels with $\text{BR} \lesssim 1\%$ have a negligible impact

on the results.

Dilepton: An opposite-sign lepton pair ($\ell^+ \ell^-$) can be produced from a RHN pair when both decay via the $W\ell$ channel. This channel does not involve missing transverse energy, making it fully reconstructible. The hadronic decays of the W bosons can result in two fatjets. The various production channels contributing to dilepton final states are as follows:

$$pp \rightarrow \left\{ \begin{array}{l} \ell_q \ell_q \\ \ell_q \nu_R (+j) \\ \nu_R \nu_R (+j) \end{array} \right\} \rightarrow \left\{ \begin{array}{l} (j\nu_R)(j\nu_R) \\ (j\nu_R)\nu_R (+j) \\ \nu_R \nu_R (+j) \end{array} \right\} \\ \rightarrow \ell^\pm W_h^\mp \ell^\mp W_h^\pm + \text{jet}(s).$$

In the dilepton channel, the dominant decay chain is $\nu_R \nu_R \rightarrow \ell^\pm W_h^\mp \ell^\mp W_h^\pm$, with an overall BR of 22%. Other channels, such as $\nu_R \nu_R \rightarrow \nu_\ell (Z_h + H_h) \nu_\ell Z_\ell$, have a BR of approximately 1% and contribute negligibly to the results. To suppress the Drell-Yan dilepton background, a Z-veto cut is applied, which effectively eliminates contributions from these subdominant processes. Consequently, our analysis focuses on the most dominant signals. Including subdomi-

TABLE III. Selection criteria applied on the monoelectron and dielectron final states.

Selection Cuts	Channels	
	Monoelectron	Dielectron
C1	$p_T(e) > 250 \text{ GeV}$ $p_T(j_1), p_T(j_2) > 110 \text{ GeV}$	$p_T(e) > 120 \text{ GeV}$ No b -tagged jet
C2	$p_T(J_1) > 350 \text{ GeV},$ $\eta(J_1) < 2.5$ $0.03 < \tau_{21}(J_1) < 0.4$	$p_T(J_1) > 280 \text{ GeV},$ $\eta(J_1) < 2.5$
C3		$M(e_1, e_2) > 250 \text{ GeV}$ $M(J_1, e_1) > 450 \text{ GeV}$
C4	$E_T^{\cancel{e}} > 180 \text{ GeV}$ $S_T > 900 \text{ GeV}$	$S_T > 1200 \text{ GeV}$

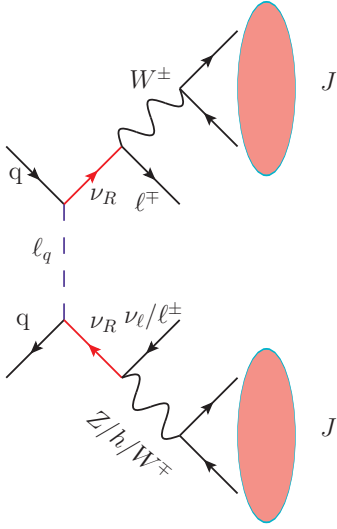


FIG. 3. Mono- and di-lepton productions at the LHC.

nant processes would not significantly affect the exclusion limits and is therefore omitted.

There are existing searches for dilepton final states via RHNs [11–13, 55, 56]. These studies are primarily motivated by the Type-I seesaw models, where RHNs are purely Majorana in nature, leading to same-sign dilepton final states with lepton number violation. In contrast, this analysis considers RHNs within the framework of the inverse seesaw mechanism, where RHNs are pseudo-Dirac in nature, resulting in opposite-sign dilepton final states.

Trilepton: Final states with both symmetric and anti-symmetric decays of the RHN pair can result in trilepton signatures. The production and decay processes leading

to these final states are as follows:

$$pp \rightarrow \left\{ \begin{array}{l} \ell_q \ell_q \\ \ell_q \nu_R (+j) \\ \nu_R \nu_R (+j) \end{array} \right\} \rightarrow \left\{ \begin{array}{l} (j \nu_R)(j \nu_R) \\ (j \nu_R) \nu_R (+j) \\ \nu_R \nu_R (+j) \end{array} \right\} \\ \rightarrow \left\{ \begin{array}{l} \ell^\pm W_\ell^\mp \ell^\pm W_\ell^\pm + \text{jet}(s) \\ \ell^\pm W_h^\mp \nu_\ell Z_\ell + \text{jet}(s) \end{array} \right\}.$$

Here, the subscript ℓ to W or Z corresponds to their leptonic decays. Similar trilepton final states through a pair of RHN can arise from the decay of a heavy neutral gauge boson or a scalar. These channels have been explored in detail in Refs. [57–59].

Four lepton: Pair of RHNs can also decay to give four lepton final states as:

$$pp \rightarrow \left\{ \begin{array}{l} \ell_q \ell_q \\ \ell_q \nu_R (+j) \\ \nu_R \nu_R (+j) \end{array} \right\} \rightarrow \left\{ \begin{array}{l} (j \nu_R)(j \nu_R) \\ (j \nu_R) \nu_R (+j) \\ \nu_R \nu_R (+j) \end{array} \right\} \\ \rightarrow \left\{ \begin{array}{l} \ell^\pm W_\ell^\mp \ell^\pm W_\ell^\pm + \text{jet}(s) \\ \nu_\ell Z_\ell \nu_\ell Z_\ell + \text{jet}(s) \end{array} \right\}.$$

This channel suffers from the small leptonic BR. Since the four-lepton SM background is small, this channel can still be accessible at the HL-LHC. Similar channels have been analysed in the context of $U(1)_{B-L}$ model in Ref. [60].

Displaced Vertex: RHN can exhibit displaced vertex signatures if its decay width is sufficiently small. In that case, the search strategy differs significantly from that for prompt decays. The decay width of RHNs depends on their mass and the mixing angle with the SM neutrinos. Displaced vertex signatures have been presented in Refs. [61–63] in the context of $Z' \rightarrow \nu_R \nu_R$ decay and in Refs. [64, 65] in the context of $\phi \rightarrow \nu_R \nu_R$ decay. In extreme scenarios, the decay width of the RHN may become so small that it decays outside the detector, leading to missing energy in the event. Such cases require a separate analysis tailored to identifying missing energy signals.

Fatjet with MET: There are also non-leptonic channels involving one or more fatjets accompanied by missing en-

TABLE IV. Cutflow for various background and signal contributions in the monoelectron and dielectron final states. We present the number of surviving events after the selection cuts for the 14 TeV 3 ab^{-1} HL-LHC (in parentheses, we present the corresponding numbers for νLQs). Two benchmark points are considered to highlight the dominance of IP at higher LQ masses.

Monoelectron final state	Selection Cuts			
	C1	C2	C3	C4
Signal benchmarks				
$M_{S_1(U_1)} = 1500 \text{ GeV}, M_{V_R} = 500 \text{ GeV}$ (PP)	30(160)	28(148)	28(148)	22(119)
$M_{S_1(U_1)} = 1500 \text{ GeV}, M_{V_R} = 500 \text{ GeV}$ (SP)	511(4613)	471(4230)	471(4230)	334(3244)
$M_{S_1(U_1)} = 1500 \text{ GeV}, M_{V_R} = 500 \text{ GeV}$ (IP)	184(3209)	133(2292)	133(2292)	82(1437)
	Total number of signal events:			438(4800)
$M_{S_1(U_1)} = 2500 \text{ GeV}, M_{V_R} = 500 \text{ GeV}$ (PP)	$< 1(< 1)$	$< 1(< 1)$	$< 1(< 1)$	$< 1(< 1)$
$M_{S_1(U_1)} = 2500 \text{ GeV}, M_{V_R} = 500 \text{ GeV}$ (SP)	17(116)	16(111)	16(111)	12(89)
$M_{S_1(U_1)} = 2500 \text{ GeV}, M_{V_R} = 500 \text{ GeV}$ (IP)	50(561)	36(416)	36(416)	24(285)
	Total number of signal events:			36(374)
Background processes				
$W_e(+2j)$	1.744×10^6	1.01×10^6	1.01×10^6	175326
$t_e t_h(+2j)$	387878	302625	30262	50557
$W_e W_j(+2j)$	30830	22383	22383	5791
$W_e Z_h(+2j)$	14474	10889	10889	2382
$t_e W_h + t_h W_e$	38503	22787	22787	2258
$t_e b$	6849	5502	5502	831
$t_e j$	161	131	131	21
	Total number of background events:			237166
Dielectron final state	Selection Cuts			
	C1	C2	C3	C4
Signal benchmarks				
$M_{S_1(U_1)} = 1500 \text{ GeV}, M_{V_R} = 500 \text{ GeV}$ (PP)	15(136)	15(136)	13(125)	13(125)
$M_{S_1(U_1)} = 1500 \text{ GeV}, M_{V_R} = 500 \text{ GeV}$ (SP)	285(2768)	284(2764)	230(2522)	228(2516)
$M_{S_1(U_1)} = 1500 \text{ GeV}, M_{V_R} = 500 \text{ GeV}$ (IP)	182(2478)	177(2317)	150(2016)	117(1518)
	Total number of signal events:			358(4159)
$M_{S_1(U_1)} = 2500 \text{ GeV}, M_{V_R} = 500 \text{ GeV}$ (PP)	$< 1(< 1)$	$< 1(< 1)$	$< 1(< 1)$	$< 1(< 1)$
$M_{S_1(U_1)} = 2500 \text{ GeV}, M_{V_R} = 500 \text{ GeV}$ (SP)	11(91)	11(91)	9(86)	9(86)
$M_{S_1(U_1)} = 2500 \text{ GeV}, M_{V_R} = 500 \text{ GeV}$ (IP)	40(441)	38(423)	33(372)	26(310)
	Total number of signal events:			35(396)
Background processes				
$(Z/\gamma^*)_e(+2j)$	253822	98786	51136	9065
$t_e t_e(+2j)$	23964	10523	6301	622
$W_e W_e(+2j)$	6159	3216	1909	494
$W_h Z_e(+2j)$	772	519	324	138
$t_e W_e$	2276	981	470	83
$Z_e Z_h(+2j)$	130	63	32	8
	Total number of background events:			10410

TABLE V. Model-independent (i.e. only PP with pure QCD taking $x \rightarrow 0$) mass limits on vLQs in GeVs for two different κ values. These numbers are obtained for the HL-LHC.

vLQ	Monoelectron				Dielectron			
	$\kappa = 1$		$\kappa = 0$		$\kappa = 1$		$\kappa = 0$	
	5σ	2σ	5σ	2σ	5σ	2σ	5σ	2σ
U_1	1160	1190	1315	1450	1269	1373	1553	1697
\bar{U}_1	1160	1190	1315	1450	1269	1373	1553	1697
\tilde{V}_2	1185	1300	1400	1622	1346	1537	1651	1833

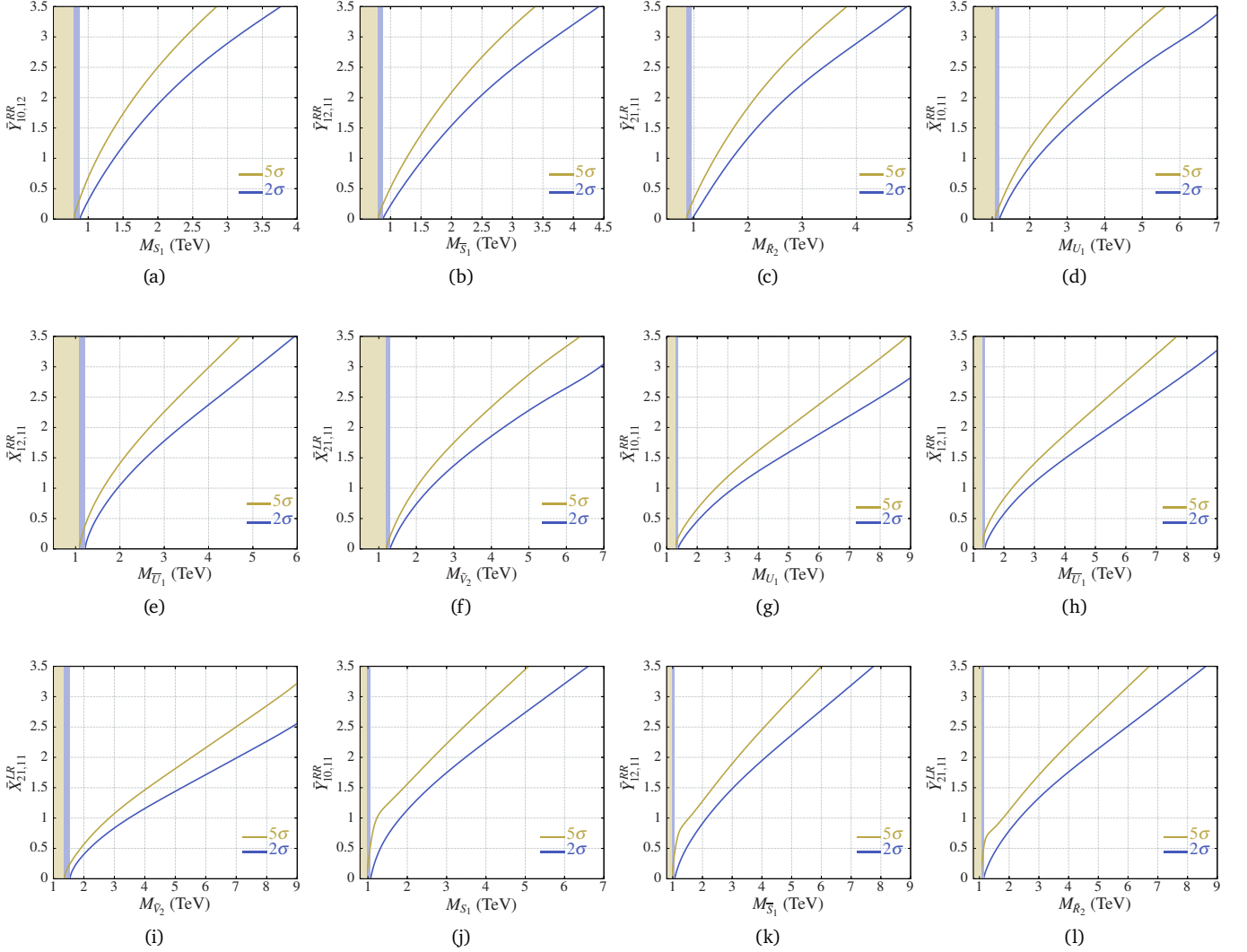


FIG. 4. The 2σ exclusion and 5σ discovery regions for sLQs and vLQs for the HL-LHC: Plots [(a)–(f)] present the monoelectron channel results, while plots [(g)–(l)] correspond to the dielectron channel results. The vertical shaded regions indicate the model-independent limits (i.e. only PP with pure QCD taking $x/y \rightarrow 0$) for different LQs. All these limits are obtained for $M_{V_R} = 500$ GeV. For vLQs, we set $\kappa = 1$ for these plots.

ergy as follows

$$\begin{aligned}
 PP \rightarrow \left\{ \begin{array}{l} \ell_q \ell_q \\ \ell_q \nu_R (+j) \\ \nu_R \nu_R (+j) \end{array} \right\} &\rightarrow \left\{ \begin{array}{l} (j\nu_R)(j\nu_R) \\ (j\nu_R)\nu_R (+j) \\ \nu_R \nu_R (+j) \end{array} \right\} \\
 &\rightarrow \nu_\ell (Z_h + H_h) \nu_\ell (Z_h + H_h) + \text{jet}(s).
 \end{aligned}$$

The background for this signal is expected to be very large. However, the signal can still be separable using advanced jet-substructure variables and machine-learning techniques. Similar final states have been analysed in the context of the inert Higgs doublet model in Ref. [66].

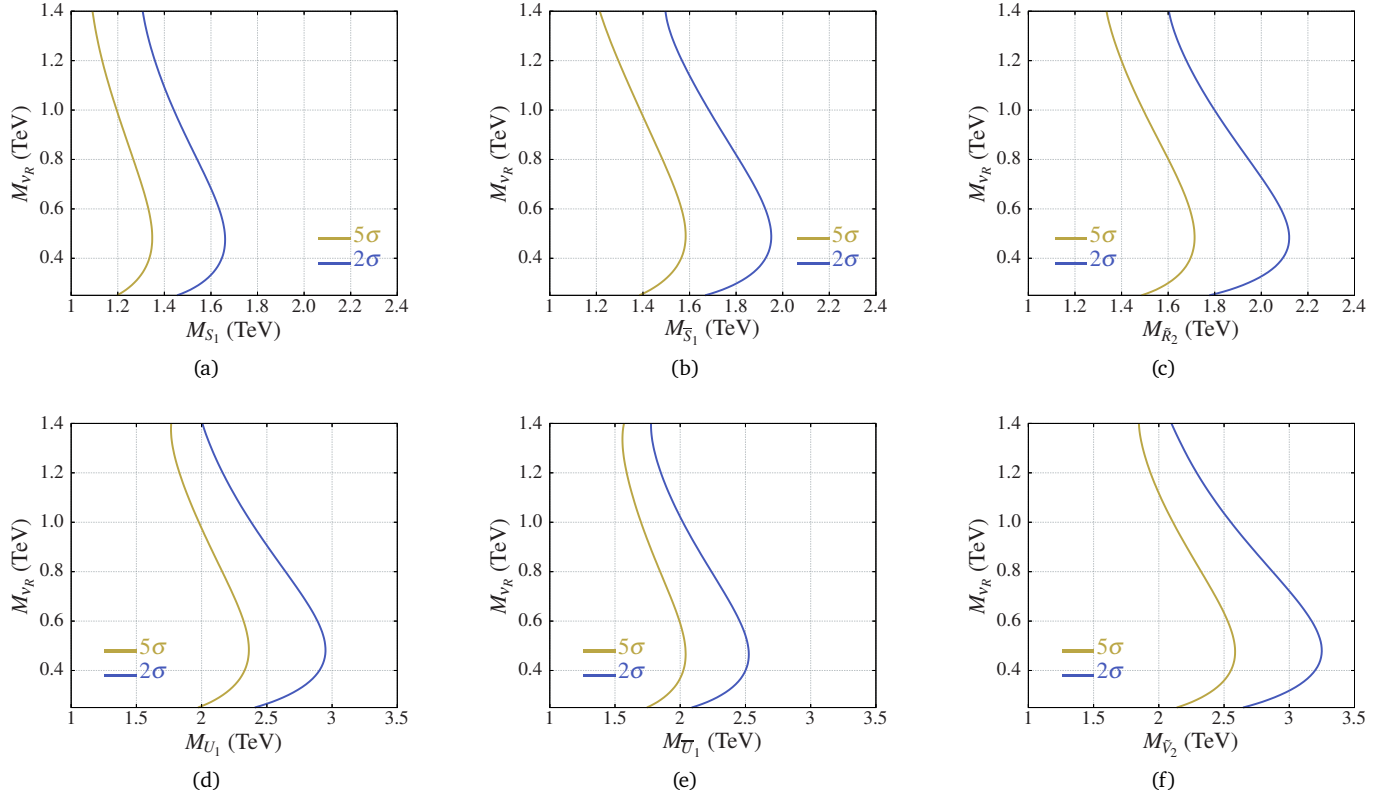


FIG. 5. The 2σ exclusion and 5σ discovery regions using the dielectron channel in the $M_{\ell_q} - M_{V_R}$ plane with fixed Coupling $x/y = 1$.

B. Signal, background and selection criteria

We focus on the first-generation LQs that decay exclusively into a first-generation quark and a first-generation RHN. Consequently, the RHN decay modes in our scenario are W_e , $Z\nu_e$, and $H\nu_e$. Our analysis focuses on the monoelectron and dielectron final states. We require at least two AK4 jets and one fatjet for the monoelectron channel. In the dielectron channel, we demand the presence of two electrons along with at least one fatjet.

The relevant SM backgrounds for our signal channels, along with their higher-order cross sections, are listed in Table II. Table III summarizes the set of cuts employed to distinguish the signal from the background. These cuts are decided by looking at various kinematic distributions for the signal and background processes. Some of the important distributions are presented in Fig. 2. In Table IV, we present the cutflow for the monoelectron and dielectron channels, showing the number of surviving signal and background events after each cut for two benchmark points for sLQ and vLQ. With the RHN mass fixed, increasing the LQ mass enhances the importance of IP, which can contribute more significantly to the total N_S compared to the combined contributions of both PP and SP. The selection cuts used to analyze the monoelectron and dielectron final states in this study differ slightly from those employed in Ref. [19], which focused on RHN production via the second-generation LQs. This difference arises because, for the first-generation LQs, the IP channel plays a

more significant role compared to the PP and the SP. Consequently, the cuts are optimised to account for kinematics that maximise event capture from the IP channel.

The dominant SM backgrounds for monoelectron and dielectron final states are $W_e + jets$ and $(Z/\gamma^*)_e + jets$ respectively, owing to their large cross-sections. Selection cuts are optimised to significantly suppress these backgrounds while retaining a substantial fraction of the signal events. The next most significant background for both channels is $tt + jets$. To mitigate this, requiring no b -tagged jets is effective, provided the signal itself contains no b -jets. In the monoelectron channel, significant contributions arise when one decays via $\nu_R \rightarrow H\nu \rightarrow bb\nu$. As a result, b -tagging is not imposed for this channel. In contrast, for the dielectron channel, where the signal does not include b -jets, we specifically require the absence of b -tagged jets to suppress backgrounds.

The fatjets in the signal primarily originate from W/Z decays, with the leading fatjet mass peaking around their masses. Consequently, applying a window-like cut around this peak can effectively reduce background contributions. However, the fatjet mass distribution for the signal exhibits a bimodal nature, with a second peak appearing at the RHN mass. Due to this characteristic, we refrain from imposing a cut on the fatjet mass in our analysis.

IV. HL-LHC PROSPECTS

For the HL-LHC (i.e., 14 TeV center-of-mass energy with $\mathcal{L} = 3 \text{ ab}^{-1}$ integrated luminosity), we estimate the number of signal events (N_S) and number of total background events (N_B) after the cuts listed in Table III. The N_S is calculated using the expression:

$$N_S = \left(\sigma_{\text{PP}} \cdot \varepsilon_{\text{PP}} + \lambda^2 \cdot \sigma_{\text{SP}} \cdot \varepsilon_{\text{SP}} + \lambda^4 \cdot \sigma_{\text{IP}} \cdot \varepsilon_{\text{IP}} \right) \cdot \mathcal{L}, \quad (2)$$

where σ_{XX} and ε_{XX} ($XX = \text{PP}, \text{SP}, \text{IP}$) are the cross section and efficiency of the signal process, with subscripts denoting different production processes. Here, λ represents the LQ coupling (x for sLQs and y for vLQs). Both σ and ε are functions of M_{ℓ_q} and M_{ν_R} , making N_S a function of these masses and λ .

To determine the 2σ exclusion or 5σ discovery sensitivity, the following \mathcal{Z} -score [67] formula is used:

$$\mathcal{Z} = \sqrt{2(N_S + N_B) \ln \left(\frac{N_S + N_B}{N_B} \right) - 2N_S}. \quad (3)$$

The results for the monoelectron and dielectron final states are presented in Fig. 4, showing 2σ exclusion and 5σ discovery contours in the $M_{\ell_q} - x(y)$ plane for sLQs (vLQs). For this analysis, the benchmark RHN mass is set to 500 GeV. The dielectron channel offers stricter exclusions compared to the monoelectron channel due to its reduced background. This improvement arises because the dominant Drell-Yan background can be significantly suppressed by applying a dielectron invariant mass cut. In Fig. 5, we show similar contours in $M_{\ell_q} - M_{\nu_R}$ plane for $\lambda = 1$ for the dielectron channel. Initially, M_{ℓ_q} increases with M_{ν_R} because the cuts are optimised for $M_{\nu_R} = 500$ GeV. For lower M_{ν_R} , the efficiency is significantly reduced, but as M_{ν_R} increases, the efficiency improves substantially, leading to a higher effective cross section. To maintain balance, M_{ℓ_q} must increase. Beyond a certain threshold of M_{ν_R} , however, the efficiency plateaus, causing M_{ℓ_q} to decrease with M_{ν_R} , as expected.

The exclusion limits for vLQs are largely insensitive to κ , as the dominant contribution arises from the IP process, which is independent of κ . Although production processes like PP and SP depend on κ , their overall impact is relatively smaller. Consequently, for larger LQ masses where the IP process dominates, the effect of κ on the derived limits remains negligible. The model-independent mass limits (i.e. only PP with $x \rightarrow 0$) for different vLQs for $\kappa = 0, 1$ are presented in Table V. Since, the cuts are op-

timised for the IP process, resulting in slightly less stringent model-independent mass limits compared to those obtained in Ref. [19]. This happens because, for low LQ masses, when the coupling x tends to zero, PP becomes the dominant production mode. However, in this case, the cuts are not optimised for the PP process.

V. SUMMARY AND CONCLUSION

We investigated the production of RHNs at the LHC, mediated by first-generation LQs. The prospects for RHN production are more promising in this case compared to the second [19] or third-generation scenarios. This is due to the enhanced PDFs of first-generation quarks, which significantly boost the production cross sections of the IP channel. We emphasised the role of the IP channel in enhancing RHN production at the LHC and designed a set of cuts optimised for this channel. While the cuts applied here are less stringent than those used for the second-generation case [19], the increased cross sections result in stricter exclusion limits. In the future, machine learning techniques could be employed to further enhance these prospects.

We derived the exclusion limits and discovery reach for the HL-LHC for all first-generation scalar and vector LQs that can produce a pair of RHNs through the pair, single and indirect production channels of LQs. Our results are presented for both the monoelectron and dielectron channels arising from the decay of RHN pairs. We found that the dielectron channel has better prospects compared to the monoelectron channel due to its lower background. The model-independent mass limits derived from the PP channel depend on the choice of the κ parameter for vLQs. However, model-dependent limits are only marginally affected by κ , as they are predominantly determined by the κ -independent IP channel.

Our study includes singlet LQs with electric charges $1/3$ and $2/3$. These limits can be directly interpreted in terms of the charge eigenstates, making the findings more accessible to experimentalists.

ACKNOWLEDGEMENT

T.M. acknowledges partial support from the SERB/ANRF, Government of India, through the Core Research Grant (CRG) No. CRG/2023/007031. R.S. acknowledges the PMRF from the Government of India.

-
- [1] P. Minkowski, $\mu \rightarrow e\gamma$ at a Rate of One Out of 10^9 Muon Decays?, *Phys. Lett. B* **67** (1977) 421–428.
[2] R. N. Mohapatra and G. Senjanovic, *Neutrino Mass and Spontaneous Parity Nonconservation*, *Phys. Rev. Lett.* **44** (1980) 912.
[3] R. N. Mohapatra, *Mechanism for Understanding Small Neutrino Mass in Superstring Theories*, *Phys. Rev. Lett.* **56**

- (1986) 561–563.
[4] R. N. Mohapatra and J. W. F. Valle, *Neutrino Mass and Baryon Number Nonconservation in Superstring Models*, *Phys. Rev. D* **34** (1986) 1642.
[5] A. M. Abdullahi et al., *The present and future status of heavy neutral leptons*, *J. Phys. G* **50** (2023) 020501, [2203.08039].

- [6] S. Banerjee, P. S. B. Dev, A. Ibarra, T. Mandal and M. Mitra, *Prospects of Heavy Neutrino Searches at Future Lepton Colliders*, *Phys. Rev. D* **92** (2015) 075002, [[1503.05491](#)].
- [7] A. Das, P. S. B. Dev and R. N. Mohapatra, *Same Sign versus Opposite Sign Dileptons as a Probe of Low Scale Seesaw Mechanisms*, *Phys. Rev. D* **97** (2018) 015018, [[1709.06553](#)].
- [8] W.-Y. Keung and G. Senjanovic, *Majorana Neutrinos and the Production of the Right-handed Charged Gauge Boson*, *Phys. Rev. Lett.* **50** (1983) 1427.
- [9] M. Thomas Arun, T. Mandal, S. Mitra, A. Mukherjee, L. Priya and A. Sampath, *Testing left-right symmetry with an inverse seesaw mechanism at the LHC*, *Phys. Rev. D* **105** (2022) 115007, [[2109.09585](#)].
- [10] A. Ekstedt, R. Enberg, G. Ingelman, J. Löfgren and T. Mandal, *Constraining minimal anomaly free $U(1)$ extensions of the Standard Model*, *JHEP* **11** (2016) 071, [[1605.04855](#)].
- [11] A. Das, N. Okada and D. Raut, *Enhanced pair production of heavy Majorana neutrinos at the LHC*, *Phys. Rev. D* **97** (2018) 115023, [[1710.03377](#)].
- [12] A. Das, N. Okada and D. Raut, *Heavy Majorana neutrino pair productions at the LHC in minimal $U(1)$ extended Standard Model*, *Eur. Phys. J. C* **78** (2018) 696, [[1711.09896](#)].
- [13] P. Cox, C. Han and T. T. Yanagida, *LHC Search for Right-handed Neutrinos in Z' Models*, *JHEP* **01** (2018) 037, [[1707.04532](#)].
- [14] D. Choudhury, K. Deka, T. Mandal and S. Sadhukhan, *Neutrino and Z' phenomenology in an anomaly-free $U(1)$ extension: role of higher-dimensional operators*, *JHEP* **06** (2020) 111, [[2002.02349](#)].
- [15] K. Deka, T. Mandal, A. Mukherjee and S. Sadhukhan, *Leptogenesis in an anomaly-free $U(1)$ extension with higher-dimensional operators*, *Nucl. Phys. B* **991** (2023) 116213, [[2105.15088](#)].
- [16] A. Das, T. Mandal, T. Nomura and S. Shil, *Heavy Majorana neutrino pair production from Z' at hadron and lepton colliders*, *Phys. Rev. D* **105** (2022) 095031, [[2202.13358](#)].
- [17] M. T. Arun, A. Chatterjee, T. Mandal, S. Mitra, A. Mukherjee and K. Nivedita, *Search for the Z' boson decaying to a right-handed neutrino pair in leptophobic $U(1)$ models*, *Phys. Rev. D* **106** (2022) 095035, [[2204.02949](#)].
- [18] J. L. Evans and N. Nagata, *Signatures of Leptoquarks at the LHC and Right-handed Neutrinos*, *Phys. Rev. D* **92** (2015) 015022, [[1505.00513](#)].
- [19] A. Bhaskar, Y. Chaurasia, K. Deka, T. Mandal, S. Mitra and A. Mukherjee, *Right-handed neutrino pair production via second-generation leptoquarks*, *Phys. Lett. B* **843** (2023) 138039, [[2301.11889](#)].
- [20] J. C. Pati and A. Salam, *Unified Lepton-Hadron Symmetry and a Gauge Theory of the Basic Interactions*, *Phys. Rev. D* **8** (1973) 1240–1251.
- [21] J. C. Pati and A. Salam, *Lepton Number as the Fourth Color*, *Phys. Rev. D* **10** (1974) 275–289. [Erratum: *Phys.Rev.D* **11**, 703–703 (1975)].
- [22] H. Georgi and S. L. Glashow, *Unity of All Elementary Particle Forces*, *Phys. Rev. Lett.* **32** (1974) 438–441.
- [23] H. Fritzsch and P. Minkowski, *Unified Interactions of Leptons and Hadrons*, *Annals Phys.* **93** (1975) 193–266.
- [24] B. Schrempp and F. Schrempp, *LIGHT LEPTOQUARKS*, *Phys. Lett. B* **153** (1985) 101–107.
- [25] M. Kohda, H. Sugiyama and K. Tsumura, *Lepton number violation at the LHC with leptoquark and diquark*, *Phys. Lett. B* **718** (2013) 1436–1440, [[1210.5622](#)].
- [26] S. Dimopoulos and L. Susskind, *Mass Without Scalars*, *Nucl. Phys. B* **155** (1979) 237–252.
- [27] E. Farhi and L. Susskind, *Technicolor*, *Phys. Rept.* **74** (1981) 277.
- [28] R. Barbier et al., *R-parity violating supersymmetry*, *Phys. Rept.* **420** (2005) 1–202, [[hep-ph/0406039](#)].
- [29] U. Aydemir, T. Mandal, S. Mitra and S. Munir, *An economical model for B-flavour and a_μ anomalies from $SO(10)$ grand unification*, [2209.04705](#).
- [30] A. Bhaskar, A. A. Madathil, T. Mandal and S. Mitra, *Combined explanation of W-mass, muon $g-2$, $RK^{(*)}$ and $RD^{(*)}$ anomalies in a singlet-triplet scalar leptoquark model*, *Phys. Rev. D* **106** (2022) 115009, [[2204.09031](#)].
- [31] A. Bhaskar, D. Das, S. Kundu, A. A. Madathil, T. Mandal and S. Mitra, *Vector leptoquark contributions to lepton dipole moments*, [2408.11798](#).
- [32] A. Bhaskar, A. Das, T. Mandal, S. Mitra and R. Sharma, *Fresh look at the LHC limits on scalar leptoquarks*, *Phys. Rev. D* **109** (2024) 055018, [[2312.09855](#)].
- [33] I. Doršner, S. Fajfer, A. Greljo, J. F. Kamenik and N. Košnik, *Physics of leptoquarks in precision experiments and at particle colliders*, *Phys. Rept.* **641** (2016) 1–68, [[1603.04993](#)].
- [34] J. Blumlein, E. Boos and A. Kryukov, *Leptoquark pair production in hadronic interactions*, *Z. Phys. C* **76** (1997) 137–153, [[hep-ph/9610408](#)].
- [35] J. Blümlein and E. Boos, *Leptoquark production at high energy e^+e^- colliders*, *Nucl. Phys. B Proc. Suppl.* **37** (1994) 181–192.
- [36] S. Catani, L. Cieri, G. Ferrera, D. de Florian and M. Grazzini, *Vector boson production at hadron colliders: A fully exclusive qcd calculation at next-to-next-to-leading order*, *Phys. Rev. Lett.* **103** (Aug, 2009) 082001.
- [37] G. Balossini, G. Montagna, C. M. Carloni Calame, M. Moretti, O. Nicrosini, F. Piccinini et al., *Combination of electroweak and qcd corrections to single w production at the fermilab tevatron and the cern lhc*, *Journal of High Energy Physics* **2010** (Jan., 2010) .
- [38] J. M. Campbell, R. K. Ellis and C. Williams, *Vector boson pair production at the lhc*, *Journal of High Energy Physics* **2011** (July, 2011) .
- [39] N. Kidonakis, *Theoretical results for electroweak-boson and single-top production*, *PoS DIS2015* (2015) 170, [[1506.04072](#)].
- [40] C. Muselli, M. Bonvini, S. Forte, S. Marzani and G. Ridolfi, *Top Quark Pair Production beyond NNLO*, *JHEP* **08** (2015) 076, [[1505.02006](#)].
- [41] A. Kulesza, L. Motyka, D. Schwartzländer, T. Stebel and V. Theeuwes, *Associated production of a top quark pair with a heavy electroweak gauge boson at NLO+NNLL accuracy*, *Eur. Phys. J. C* **79** (2019) 249, [[1812.08622](#)].
- [42] A. Alloul, N. D. Christensen, C. Degrande, C. Duhr and B. Fuks, *FeynRules 2.0 - A complete toolbox for tree-level phenomenology*, *Comput. Phys. Commun.* **185** (2014) 2250–2300, [[1310.1921](#)].
- [43] J. Alwall, R. Frederix, S. Frixione, V. Hirschi, F. Maltoni, O. Mattelaer et al., *The automated computation of tree-level and next-to-leading order differential cross sections, and their matching to parton shower simulations*, *JHEP* **07** (2014) 079, [[1405.0301](#)].
- [44] **NNPDF** collaboration, R. D. Ball et al., *An open-source machine learning framework for global analyses of parton distributions*, *Eur. Phys. J. C* **81** (2021) 958, [[2109.02671](#)].

- [45] M. Kramer, T. Plehn, M. Spira and P. M. Zerwas, *Pair production of scalar leptoquarks at the CERN LHC*, *Phys. Rev. D* **71** (2005) 057503, [[hep-ph/0411038](#)].
- [46] T. Mandal, S. Mitra and S. Seth, *Pair Production of Scalar Leptoquarks at the LHC to NLO Parton Shower Accuracy*, *Phys. Rev. D* **93** (2016) 035018, [[1506.07369](#)].
- [47] C. Borschensky, B. Fuks, A. Kulesza and D. Schwartländer, *Scalar leptoquark pair production at hadron colliders*, *Phys. Rev. D* **101** (2020) 115017, [[2002.08971](#)].
- [48] C. Borschensky, B. Fuks, A. Kulesza and D. Schwartländer, *Scalar leptoquark pair production at the LHC: precision predictions in the era of flavour anomalies*, *JHEP* **02** (2022) 157, [[2108.11404](#)].
- [49] C. Borschensky, B. Fuks, A. Kulesza and D. Schwartländer, *Precision predictions for scalar leptoquark pair production at the LHC*, *PoS EPS-HEP2021* (2022) 637, [[2110.15324](#)].
- [50] C. Borschensky, B. Fuks, A. Jueid and A. Kulesza, *Scalar leptoquarks at the LHC and flavour anomalies: a comparison of pair-production modes at NLO-QCD*, *JHEP* **11** (2022) 006, [[2207.02879](#)].
- [51] C. Bierlich et al., *A comprehensive guide to the physics and usage of PYTHIA 8.3*, *SciPost Phys. Codeb.* **2022** (2022) 8, [[2203.11601](#)].
- [52] DELPHES 3 collaboration, J. de Favereau, C. Delaere, P. Demin, A. Giammanco, V. Lemaître, A. Mertens et al., *DELPHES 3, A modular framework for fast simulation of a generic collider experiment*, *JHEP* **02** (2014) 057, [[1307.6346](#)].
- [53] M. Cacciari, G. P. Salam and G. Soyez, *FastJet User Manual*, *Eur. Phys. J. C* **72** (2012) 1896, [[1111.6097](#)].
- [54] M. Cacciari, G. P. Salam and G. Soyez, *The anti- k_r jet clustering algorithm*, *JHEP* **04** (2008) 063, [[0802.1189](#)].
- [55] S. Chakdar, K. Ghosh, V. Hoang, P. Q. Hung and S. Nandi, *Search for electroweak-scale right-handed neutrinos and mirror charged leptons through like-sign dilepton signals*, *Phys. Rev. D* **95** (Jan, 2017) 015014.
- [56] J. N. Ng, A. de la Puente and B. W.-P. Pan, *Search for Heavy Right-Handed Neutrinos at the LHC and Beyond in the Same-Sign Same-Flavor Leptons Final State*, *JHEP* **12** (2015) 172, [[1505.01934](#)].
- [57] Z. Kang, P. Ko and J. Li, *New avenues to heavy right-handed neutrinos with pair production at hadronic colliders*, *Phys. Rev. D* **93** (Apr, 2016) 075037.
- [58] E. Accomando, L. Delle Rose, S. Moretti, E. Olaiya and C. H. Shepherd-Themistocleous, *Extra Higgs boson and Z' as portals to signatures of heavy neutrinos at the LHC*, *JHEP* **02** (2018) 109, [[1708.03650](#)].
- [59] J. C. Helo, H. Li, N. A. Neill, M. Ramsey-Musolf and J. C. Vasquez, *Probing neutrino Dirac mass in left-right symmetric models at the LHC and next generation colliders*, *Phys. Rev. D* **99** (2019) 055042, [[1812.01630](#)].
- [60] K. Huitu, S. Khalil, H. Okada and S. K. Rai, *Signatures for right-handed neutrinos at the large hadron collider*, *Phys. Rev. Lett.* **101** (Oct, 2008) 181802.
- [61] F. F. Deppisch, S. Kulkarni and W. Liu, *Heavy neutrino production via Z' at the lifetime frontier*, *Phys. Rev. D* **100** (Aug, 2019) 035005.
- [62] C.-W. Chiang, G. Cottin, A. Das and S. Mandal, *Displaced heavy neutrinos from Z' decays at the LHC*, *JHEP* **12** (2019) 070, [[1908.09838](#)].
- [63] A. Das, P. B. Dev and N. Okada, *Long-lived tev-scale right-handed neutrino production at the lhc in gauged $u(1)_x$ model*, *Physics Letters B* **799** (2019) 135052.
- [64] F. F. Deppisch, W. Liu and M. Mitra, *Long-lived Heavy Neutrinos from Higgs Decays*, *JHEP* **08** (2018) 181, [[1804.04075](#)].
- [65] W. Liu, J. Li, J. Li and H. Sun, *Testing the seesaw mechanisms via displaced right-handed neutrinos from a light scalar at the HL-LHC*, *Phys. Rev. D* **106** (2022) 015019, [[2204.03819](#)].
- [66] A. Bhardwaj, P. Konar, T. Mandal and S. Sadhukhan, *Probing the inert doublet model using jet substructure with a multivariate analysis*, *Phys. Rev. D* **100** (2019) 055040, [[1905.04195](#)].
- [67] G. Cowan, K. Cranmer, E. Gross and O. Vitells, *Asymptotic formulae for likelihood-based tests of new physics*, *Eur. Phys. J. C* **71** (2011) 1554, [[1007.1727](#)]. [Erratum: *Eur.Phys.J.C* 73, 2501 (2013)].